第 34 卷第 8 期 无 机 化 学 学 报 Vol.34 No.8
2018 年 8 月 CHINESE JOURNAL OF INORGANIC CHEMISTRY 1581-1589

碳包覆 $LiFe_{0.5}Co_{0.5}PO_4$ 固溶体正极材料的制备及其电化学性能

钟艳君 吴振国 田 海 郭孝东 钟本和 王辛龙*
(四川大学化学工程学院,成都 610065)

摘要: 分别以四水磷酸铁($FePO_4·4H_2O$)和二水草酸亚铁($FeC_2O_4·2H_2O$)为铁源,采用简单便捷的流变相法制备了碳包覆 $LiFe_{0.5}Co_{0.5}PO_4$ 固溶体材料($LiFe_{0.5}Co_{0.5}PO_4/C$,简称为 LFCP/C)。采用 X 射线衍射(XRD)、扫描电镜(SEM)、透射电镜(TEM)、恒流充放电等测试手段对复合材料的物相、形貌结构和电化学性能进行了表征和测试。结果表明,2 种铁源得到的材料均为橄榄石晶型结构且结晶度良好,二者在颗粒尺寸分布、碳包覆效果和电化学性能方面具有显著的差别。用作锂离子电池正极材料时,以 $FeC_2O_4·2H_2O$ 为原料得到的 LFCP/C 具有更优异的电性能:在 2.5~5.0 V 电压范围内,0.1C 倍率下(1C=150 $mA·g^{-1}$),放电比容量为 137.5 $mAh·g^{-1}$,在 10C 仍具有 57.6 $mAh·g^{-1}$ 的放电比容量;0.5C 循环 100 次后容量仍保持 78.1%。该样品更佳的电化学性能主要得益于其更小的平均颗粒尺寸,更高的比表面积和理想的碳包覆效果。

关键词: 锂离子电池; $LiFe_{0.5}Co_{0.5}PO_4/C$; 流变相法; 铁源; 电化学性能
中图分类号: O646 **文献标识码**: A **文章编号**: 1001-4861(2018)08-1581-09
DOI: 10.11862/CJIC.2018.192

Synthesis and Electrochemical Performances of Carbon Coated $LiFe_{0.5}Co_{0.5}PO_4$ Solid Solution as Cathode Materials

ZHONG Yan-Jun WU Zhen-Guo TIAN Hai GUO Xiao-Dong ZHONG Ben-He WANG Xin-Long*
(*School of Chemical Engineering, Sichuan University, Chengdu* 610065, *China*)

Abstract: Cabon coated $LiFe_{0.5}Co_{0.5}PO_4$ solid solution ($LiFe_{0.5}Co_{0.5}PO_4/C$, LFCP/C) were synthesized via a facile rheological phase method using iron phosphate tetrahydrate ($FePO_4·4H_2O$) and iron oxalate dihydrate ($FeC_2O_4·2H_2O$) as iron source, respectively. The phase composition, particle morphology and electrochemical performance for the as-prepared materials were characterized by methods including X-ray diffraction (XRD), scanning electron microscope (SEM), transmission electron microscope (TEM) and galvanostatic charge-discharge measurements. Results demonstrate that both LFCP/C samples possess olivine structure with high crystallinity, while there are significant difference in particle size distribution, carbon coating effect and electrochemical properties. As cathode for lithium ion batteries (LIBs), the LFCP/C obtained by $FeC_2O_4·2H_2O$ as reactant exhibits better electrochemical performance than that by $FePO_4·4H_2O$, delivering a specific discharge capacity of 137.5 $mAh·g^{-1}$ at 0.1C (1C= 150 $mA·g^{-1}$) rate in the voltage range of 2.5~5.0 V, and even at 10C rate, a specific capacity of 57.6 $mAh·g^{-1}$ is still maintained. Meanwhile, it shows excellent cyclability with a capacity retention rate of 78.1% after 100 cycles at 0.5C. The better electrochemical performance of LFCP/C obtained by $FeC_2O_4·2H_2O$ can be mainly ascribed to its smaller average particle size, higher BET specific surface area, and more appealing carbon coating effect.

Keywords: lithium ion battery; $LiFe_{0.5}Co_{0.5}PO_4/C$; rheological phase method; iron source; electrochemical performance

收稿日期:2018-04-23。收修改稿日期:2018-05-31。
四川大学专职博士后研发基金(No.2017SCU12018)和国家重点研发计划(No.2017YFB0307504)资助项目。
*通信联系人。E-mail:wangxl@scu.edu.cn

0 Introduction

Lithium-ion batteries (LIBs) that can effectively store energy in the form of chemicals are now attracting the international community's concern for applications in portable electronic devices and electrical vehicles[1-2]. Cathode materials which determine the energy density of LIBs at one level have become a hot topic in recent years[3-5]. $LiFePO_4$, as the most famous member of the family of olivine-type lithium transition metal phosphates ($LiMPO_4$, M=Fe, Mn, Co, Ni), is quite attractive for the cathodes of LIBs due to its good stability, low cost, and abundant in nature[6-9]. However, its relatively low potential of 3.45 V (vs Li^+/Li, as below) would restrict its further application because of the ever-increasing demand for efficient energy storage systems in hybrid electric vehicles and plugin hybrid electric vehicles. $LiCoPO_4$ also has been attracted much attention for its high working potential (4.8 V) at the stability limit of the carbonate-based liquid electrolytes and its small lattice volume change (~2%) during charge/discharge processes between the $CoPO_4$ and $LiCoPO_4$ compounds[10-12]. Nevertheless, remarkable capacity fading caused by structure deterioration and electrolyte decomposition limit its practical application. Thus, it would be of momentous importance if it can combine the excellent cycling behaviour of $LiFePO_4$ and the high operation voltage of $LiCoPO_4$. In fact, olivine solid solutions especially $LiFe_{1-x}Mn_xPO_4$ has been investigated intensively in recent years [13-16]. Inspired by this, the binary olivine $LiFe_xCo_{1-x}PO_4$ compounds which are scarcely reported, would be worth studying.

The electrochemical performances of olivine $LiMPO_4$ are usually limited by the poor electronic conductivity and low Li-ion mobility. Various methods have been attempted to improve the battery performance of lithium iron phosphate. Among them, it is facile and efficient to composite the $LiMPO_4$ with carbon nanomaterials[17-19]. Carbon nanomaterials usually serve as a conductive agent to improve the electrical conductivity while increasing the material porosity in which the solid-state diffusion distances are significantly shortened [20-23]. According to our knowledge, the nanostructure and carbon coating effects about $LiFe_xCo_{1-x}PO_4$ component seem to have received less attention among the few previous reports[24-26]. Based on the previous reports, the carbon layer is more difficult to be coated on the surface of $LiCoPO_4$ than other olivine-structured compounds like $LiFePO_4$, which may be associated with the distinct surface features of $LiCoPO_4$[27-28]. This could make it more challenging to get a well carbon coated $LiFe_xCo_{1-x}PO_4$ solid solution composite with full and homogeneous carbon coverage. As demonstrated in previous reports[29-31], it is easily obtain nanomaterials with desired carbon coating via rheological phase method, for it ensures improved quality of mixing and optimized element and particle size distributions. Besides, the heat and mass transfer between the solid particle and fluid can be carried out easily and quickly in the solid-liquid rheological mixture[32-34]. In our previous works[29,35-37], we successfully used the rheological phase method to synthesize $LiMn_{0.5}Fe_{0.5}PO_4$/C, $Li_3V_2(PO_4)_3$/C, $LiFe_{0.5}Mn_{0.3}Co_{0.2}PO_4$/C composites.

In current study, we have reported the preparation of $LiFe_{0.5}Co_{0.5}PO_4$/C (LFCP/C) composite by a facile rheological phase method and evaluated their electrochemical performances as cathode materials for LIBs. Based on the results from SEM and TEM, it is clearly proved that the LFCP/C sample synthesized via $FeC_2O_4\cdot 2H_2O$ exhibits smaller particles size, better dispersion and more favorable carbon coating effect than the one by $FePO_4\cdot 4H_2O$, thus leading to the more excellent Li-storage capability.

1 Experimental

1.1 Material syntheses

The carbon decorated $LiFe_{0.5}Co_{0.5}PO_4$/C (denoted as LFCP/C) samples were synthesized by rheological phase method. In a typical synthesis for 0.02 mol of LFCP/C product, stoichiometric amount of Li_2CO_3, $FePO_4\cdot 4H_2O$ or $FeC_2O_4\cdot 2H_2O$, $CoCO_3$ and $NH_4H_2PO_4$ as raw materials, 2 g of stearic acid as carbon source, and 6 mL of ethylalcohol (AR) as grinding aid were used. After planetary ball milling at 500 $r\cdot min^{-1}$ for 10 h, the obtained rheological mixture was preheated

at 400 ℃ for 5 h and then sintered at 600 ℃ for 10 h in a tube furnace with argon as the shielding gas to yield the LFCP/C product. The LFCP/C composites via $FePO_4 \cdot 4H_2O$ and $FeC_2O_4 \cdot 2H_2O$ are correspondingly labeled as LFCP/C-FP and LFCP/C-FO, respectively.

1.2 Material characterization

Powder X-ray diffraction (XRD) measurement was performed on Rigaku Ultima Ⅳ device using Cu $K\alpha$ radiation (λ=0.154 nm), operating at 35 kV×30 mA in range 2θ from 10° to 70° with the scanning speed of $5° \cdot min^{-1}$ for identification of phase as-prepared LFCP/C materials. The particle morphology of the as-prepared compounds was characterized using a field emission scanning electron microscope (FESEM, S-4800) operated 15 kV. Transmission electron microscope (TEM, JEM-2100) operated 200 kV was further used to observe the morphology structure and carbon coating effect of the samples. An automated surface area analyzer (ASAP2020, Micromeritics) based on BET method using nitrogen adsorption-desorption isotherms was employed for specific surface area measurement. The carbon content of the synthesized composite was detected by Vario EL Ⅲ Elemental analyzer (Elementar Analysen Syetem GmbH).

1.3 Electrochemical measurement

The electrochemical performance was measured using CR2025 coin cells. The positive electrode was fabricated by a mixture of active material, carbon black (CB), and LA-133 (a kind of water-soluble binder purchased from Chengdu Yin Di Le Power Technology Co., Ltd., China) with $w_{\text{active material}}:w_{CB}:w_{LA\text{-}133}$=80∶10∶10 mixed in water solution. The slurry was coated uniformly onto the aluminum foil and dried at 120 ℃ for 12 h in a vacuum oven, and then punched in model and weighed. The coin cells were assembled in an argon-filled glove box using Li metal as the anode and porous polypropylene film (Celgard 2400) as the separator. The employed high-voltage electrolyte mainly consists a solution of 1 $mol \cdot L^{-1}$ $LiPF_6$ in a solvent mixture of ethylene carbonate (EC) and dimethyl carbonate (DMC) (V_{EC}∶V_{DMC}=1∶1). The charge-discharge tests were galvanostatically performed between 2.5 and 5.0 V with various C-rates (1C=150 $mA \cdot g^{-1}$) on the battery test system (Neware BTS). The electrochemical impedance spectroscopy (EIS) was measured on a Zahner electrochemical workstation between 10 mHz to 100 kHz with the alternating current voltage (AC) voltage amplitude of 5 mV. All electrochemical tests were carried out at room temperature.

2 Results and dissolution

The XRD patterns of the as-prepared LFCP/C samples are presented in Fig.1. All diffraction characteristic peaks for the two samples are assigned to olivine structure in orthorhombic and *Pnma* (62) space group based on the standard XRD patterns of $LiFePO_4$ (PDF No.83-2092) and $LiCoPO_4$ (PDF No.85-0002). There are no impurities observed in the patterns, and the peak strength and peak position are very similar for the two samples, implying that high-purity products were obtained by both the Fe raw materials. Besides, good crystallinity can be inferred for the two samples as evidenced from the narrow and sharp peaks. Results based on elemental analyzer indicate that the residual carbon content for LFCP/C-FP and LFCP/C-FO are 2.72% and 1.98% (*w*/*w*), respectively, while no carbon peak presented in the XRD patterns because of the relatively low content and the amorphous state.

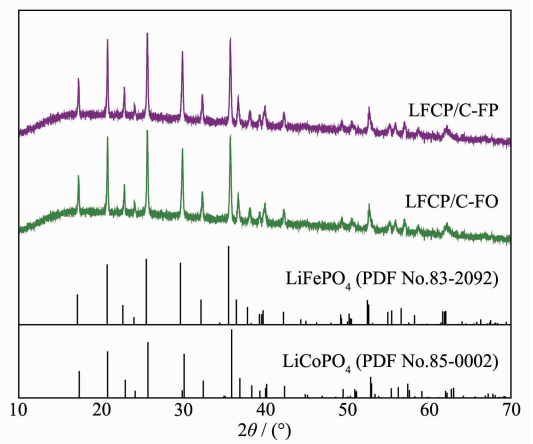

Fig.1　XRD patterns of LFCP/C samples

Fig.2 shows the SEM images for LFCP/C-FO and LFCP/C-FP. As can be clearly observed from low-magnification SEM images in Fig.2(a,e) which provide an overview of the morphology of the as-prepared products, LFCP/C-FO and LFCP/C-FP are composed

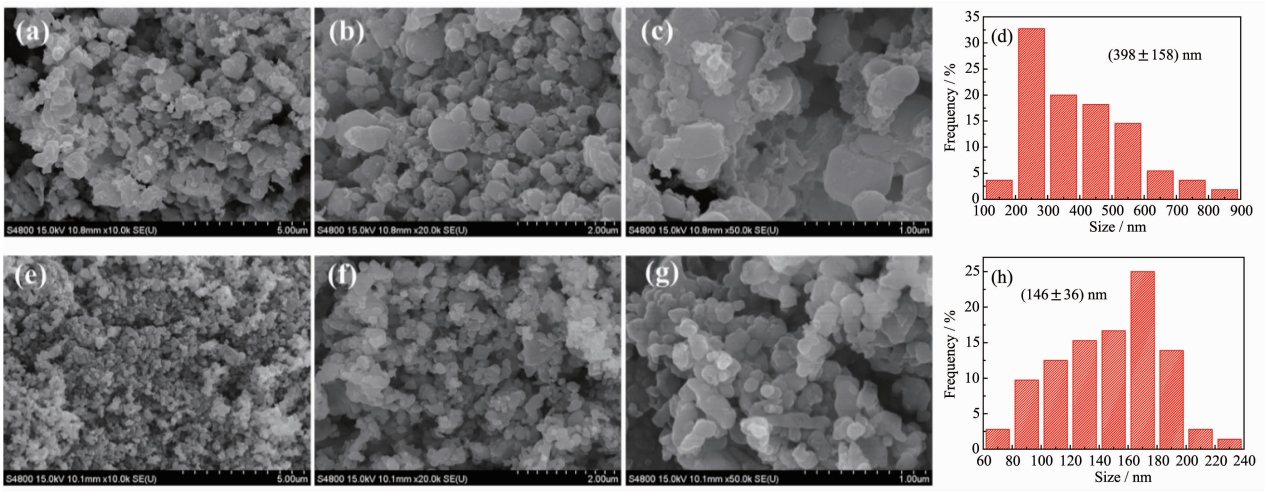

Fig.2 SEM images of (a~c) LFCP/C-FP and (e~g) LFCP/C-FO; Statistics of particle size distribution of (d) LFCP/C-FP (based on (b)) and (h) LFCP/C-FO (based on (f))

of nanoparticles, while the particles seem more serious aggregation in LFCP/C-FP evidenced by some micros-ized aggregate in the image. According to the repre-sentative high-magnification SEM images in Fig.2(b,c, f,g), both of the samples show nanoparticle morpho-logy but LFCP/C-FO seems more uniform with signifi-cantly smaller average particle size. The statistics of particle size distribution shown in Fig.2(d,h), which are respectively based on SEM images of Fig.2(b,f), also verified that LFCP/C-FO possesses a narrower particle size distribution and smaller average particle size of 146 nm than LFCP/C-PO. Furthermore, in the high-magnification SEM image of Fig.2(c) for LFCP/C-FP, some flocculent carbon is visible scattered by particles, suggesting that some carbon has not been covered on the surface of particles. Unsurprisingly, as characterized by nitrogen adsorption-desorption analy-sis, LFCP/C-FO (44 $m^2 \cdot g^{-1}$) has a higher BET specific surface area than LFCP/C-FP (23 $m^2 \cdot g^{-1}$), which could mainly be associated with the smaller particle size and higher dispersity for the former. The fundamental cause for the structural feature of LFCP/C-FO may be derived from a lot of gas generated by $FeC_2O_4 \cdot 2H_2O$ thermal decomposition in the calcination process. In general, a larger specific surface area can effectively increase the interface between electrode and electrolyte, thus enhancing an effective charge transfer across the interface[38].

To further demonstrate the difference in particle morphology and carbon coating effect of the LFCP/C samples, Fig.3 gives the TEM and HRTEM images. Fig.3(a) shows the irregular shaped aggregate of LFCP/C-FP composed by nanoparticles with an inho-mogeneous size distribution, and the serious adhesion phenomenon between particles can be observed. The surface of particle seems barely coated by carbon layer, and even some striking quilted carbon is dishe-veled around the particles, as shown in Fig.3(b). Only a small part of particles has been coated by the carbon layer effectively, such as the one shown in Fig. 3(c), where a ~2.0 nm thickness carbon layer is coated on the outer of particles. The lattice with *d*-spacing 0.301 nm and reconcilable with the lattice fringe values of (211) plane olivine structure were evident in Fig.3(c). Fig.3(d) shows LFCP/C-FO contains well-proportioned spherical or ellipsoidal particles, and the grain diameter is about 50~100 nm being coated by amorphous carbon. No stacked carbon can be observed in Fig.3(e), implying that the desired carbon coating effect has been realized in the LFCP/C-FO sample. Fig.3(f) shows that the particle is covered by a ~2.5 nm thickness carbon layer, and there are different lattice spaces of 0.253, and 0.292 nm, corresponding to (131), and (200) atomic layers of $LiFe_{0.5}Co_{0.5}PO_4$, respectively. These indicate that the particle has a well-ordered crystal structure. Previous

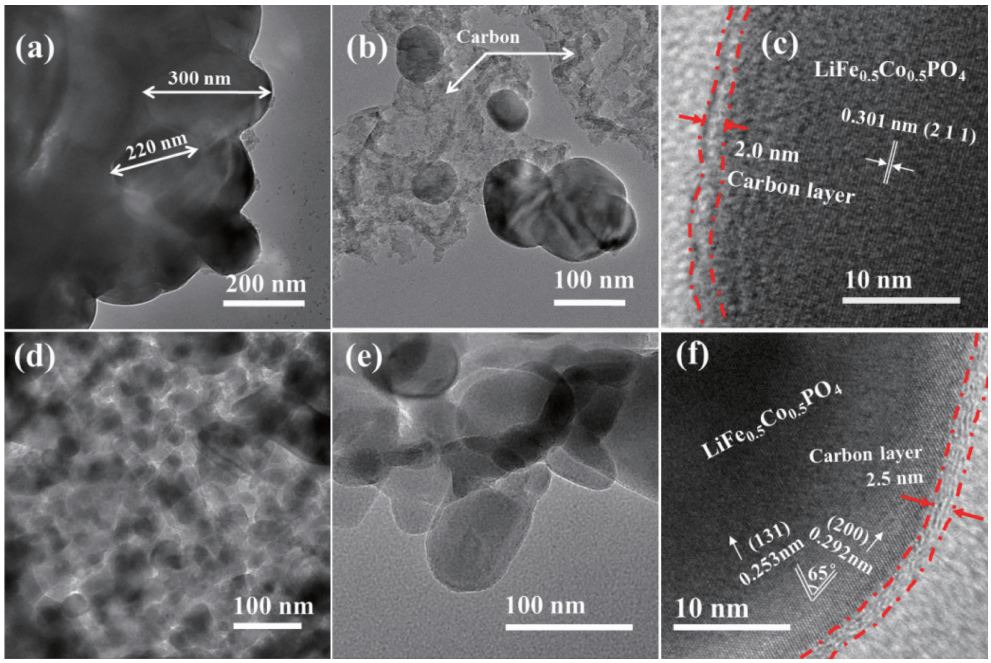

Fig.3　TEM and HRTEM images of (a~c) LFCP/C-FP and (d~f) LFCP/C-FO

researches have proven that fine carbon coating can increase the electronic conductivity of materials and buffer the mechanical damage of the active materials during the Li ion insertion/extraction process[39]. With the above analysis, it can be inferred that the LFCP/C-FO may offer better electrochemical performances.

Fig.4(a) displays galvanostatic charge/discharge voltage profiles at a current density of 0.05C between 2.5 and 5.0 V of the first and third cycles for the two cathode materials. The profiles present two reversible voltage plateaus around 3.5 and 4.8 V for the two LFCP/C samples, corresponding to the Fe^{3+}/Fe^{2+} and Co^{3+}/Co^{2+} redox, respectively. The first cycle charge and discharge profiles of LFCP/C-FP deliver specific capacities of 159.8 and 109.6 mAh·g^{-1}, respectively, with coulombic efficiency of 68.6%. As a comparison, LFCP/C-FO exhibits higher charge capacity of 201.3 mAh·g^{-1} and discharge capacity of 136.1 mAh·g^{-1}, with coulombic efficiency of 67.6%. The capacity loss more than 30% in the initial cycle for the both electrodes is mainly attributed to the electrolyte decomposition and irreversible reaction associated to Co^{2+}/Co^{3+}, which is commonly observed for high-voltage materials like $LiCoPO_4$[40-41]. Then in the third cycle, the discharge capacity increased to 119.2 mAh·g^{-1} for LFCP/C-FP and 139.9 mAh·g^{-1} for LFCP/C-FO. In addition, the coulombic efficiency reaches a value of more than 90% at the 3rd cycle for both electrodes. Furthermore, as can be observed that from the charge/discharge voltage profiles, the platform length of near 4.8 V for LFCP/C-FP is somewhat shorter than that of LFCP/C-FO while the one of ~3.4 V is similar, signifying that the lower capacity for LFCP/C-FP ought to be mainly ascribed to Co^{3+}/Co^{2+} redox reaction. This phenomenon could be associated with electrochemical activation process of LFCP/C electrodes. Fig. 4(b) shows the differential capacity profiles of the 3rd cycle for the samples. There are two cathodic/anodic peaks positioned at about 3.49/3.46 V and 4.80/4.76 V identified as Fe^{3+}/Fe^{2+} and Co^{3+}/Co^{2+} redox couple, respectively, in accordance with the charge/discharge profiles.

Rate performances of the two electrodes at different rates are shown in Fig.5(a). A relatively higher discharge capacity was found for LFCP/C-FO than LFCP/C-FP at various discharge rates. Specifically, the LFCP/C-FO electrode delivers a reversible capacity of 137.5, 129.5, 114.1, 100.0, 86.7, 73.9 and 57.6 mAh·g^{-1} at 0.1C, 0.2C, 0.5C, 1C, 3C, 5C and 10C respectively. As a comparison, the corresponding

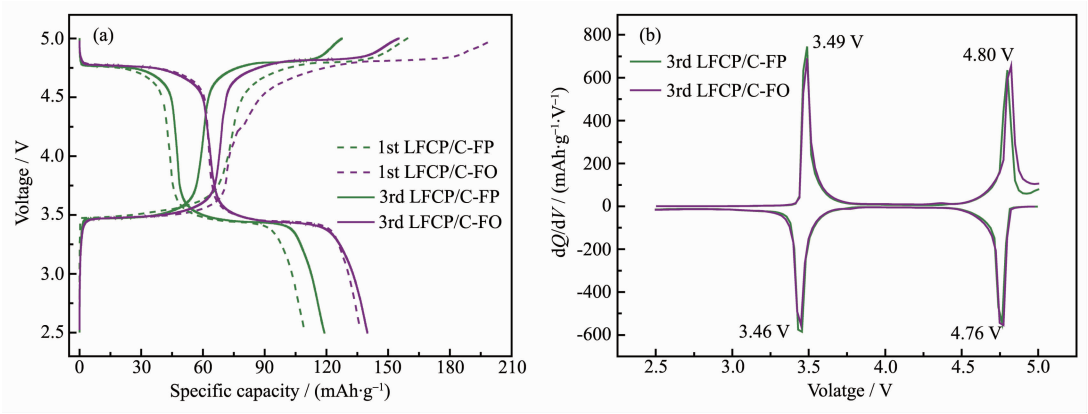

Fig.4 First and third charge/discharge curves at 0.05C (a) and the corresponding differential capacity curves in the third cycle (b) for both $LiFe_{0.5}Co_{0.5}PO_4$/C electrodes

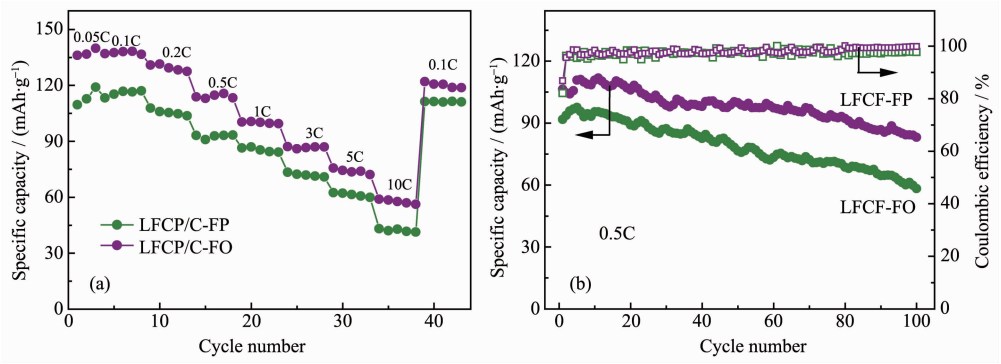

Fig.5 Electrochemical behaviors of $LiFe_{0.5}Co_{0.5}PO_4$/C electrodes: (a) Rate property and (b) cycling performance at 0.5C in the potential range of 2.5~5.0 V (vs Li^+/Li)

capacity for LFCP/C-FP is 115.8, 105.5, 92.7, 85.5, 72.0, 61.3 and 42.2 mAh·g^{-1}, respectively. When the current rate is set back to 0.1C after rate performances measurement, the capacity for LFCP/C-FO and LFCP/C-FP is 120.2 and 111.2 mAh·g^{-1}, respectively.

Fig.5(b) gives the comparison of cycling performance at 0.5C in the range of 2.5~5.0 V for the two LFCP/C electrodes. During the cycling process, the coulombic efficiency gradually increases and then steadily reaches a value higher than 98.0%, indicating the good reversibility of as-obtained LFCP/C samples. Remarkably, LFCP/C-FO shows slower capacity fading than the other one. It maintains 83.1 mAh·g^{-1} after 100 cycles with 78.1% of capacity retention ratio, in contrast, only discharge capacity of 58.3 mAh·g^{-1} and capacity retention ratio of 63.5% for LFCP-FP. These results demonstrate that LFCP/C-FO has more excellent electrochemical performance, which can be associated with the smaller particle size which shortens the diffusion distance Li^+, and the uniform and full carbon coating layer which not only enhance the electronic conductivity, but also act as a protective barrier for active materials from being severely corroded.

EIS tests were conducted to disclose the reasons for the better comprehensive electrochemical performances of LFCP/C-FO. Before the EIS tests, the cells were first charged and discharged for three cycles at 0.1C. Subsequently, the EIS tests were taken at the full discharge state of 2.5 V. Fig.6(a) gives the Nyquist plots for LFCP/C-FP and LFCP/C-FO. The small interrupt is corresponding to the solution impedance (R_e). The semicircle can be assigned to the charge transfer impedance (R_{ct}) in the high to medium frequency. The short quasi-straight line observed in the low frequency is related to the solid-state diffusion of Li^+ in the active materials, which is also called Warburg

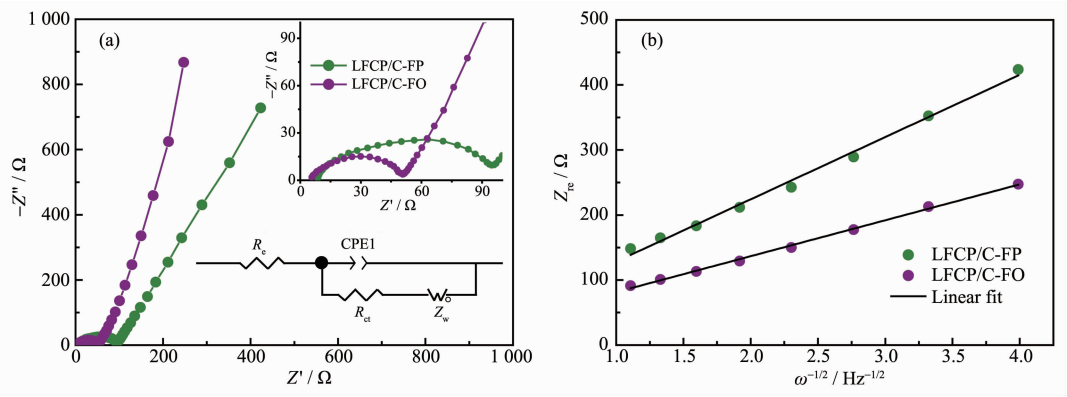

Fig.6　(a) EIS profiles of LFCP/C-FP and LFCP/C-FO samples, the inset shows an equivalent circuit; (b) Relationship between Z_{re} and $\omega^{-1/2}$ at low frequency

impedance (Z_w). The Nyquist plots are fitted by using an equivalent circuit as inserted in Fig.6(a). A constant phase element (CPE) is placed to represent the double layer capacitance and passivation film capacitance[42]. The calculated values of R_e and R_{ct} for LFCP/C-FP and LFCP/C-FO are listed in the Table 1. It seems that the R_e value of LFCP/C-FO (5.83 Ω) is similar to that of LFCP/C-FP (6.17 Ω). The main difference between these two electrodes is the charge transfer resistant (R_{ct}). The value of R_{ct} for LFCP/C-FO (48.75 Ω) is much lower than that of LFCP/C-FP (110.9 Ω), which can be attributed to the uniform and full carbon coating layer in the surfaces of primary particles. It reveals that on one side, the higher specific surface area is beneficial for the electrolyte to thoroughly contact with the particle surface, which will facilitate the Li^+ to travel from the electrolyte to the solid material. On the other side, there are still connected points between the primary particles (due to the formation of the secondary particles), resulting in a facile transfer of Li^+ and the electron in the solid active material[17,43]. Thus, it is also one of the main reasons for the improved rate capability of LFCP/C-FO. The lithium ion diffusion coefficient can be calculated according the following equations[44-45]:

$$D=(R^2T^2)/(2A^2n^4F^4C^2\sigma^2) \quad (1)$$

$$Z_{re}=R_e+R_{ct}+\sigma\omega^{-1/2} \quad (2)$$

Where D is the Li^+ diffusion coefficient ($cm^2\cdot s^{-1}$), R is the gas constant ($J\cdot mol^{-1}\cdot K^{-1}$), T is the absolute temperature (K), A is the contact area of the electrode (m^2), n is the number of the electrons per molecule, F is the Faraday constant ($C\cdot mol^{-1}$), C is the concentration of the lithium ion ($mol\cdot L^{-1}$), Z_{re} is Li^+ diffusion resistance in the electrode material (the real part of cell impedance, Ω), ω is angular frequency, and the σ is the Warburg coefficient which is equal to the slope of the straight line as illustrated in Fig.6(b). The diffusion coefficient (Table 1) is calculated to be about 2.08×10^{-14} $cm^2\cdot s^{-1}$ for LFCP/C-FP and 6.39×10^{-14} $cm^2\cdot s^{-1}$ for LFCP/C-FO, respectively. Therefore, it is reasonable to conclude that the improvement of the electrochemical reaction activity and ion diffusion are responsible for remarkable rate performance and good cycle stability of the LFCP/C-FO sample.

Table 1　Electrochemical kinetics parameters obtained from the equivalent circuit fitting of the EIS for the LFCP/C-FP and LFCP/C-FO electrodes

Sample	R_e / Ω	R_{ct} / Ω	D / ($cm^2\cdot s^{-1}$)
LFCP/C-FP	6.17	110.9	2.08×10^{-14}
LFCP/C-FO	5.83	48.75	6.39×10^{-14}

3　Conclusions

In conclusion, $LiFe_{0.5}Co_{0.5}PO_4$/C composites were prepared by a facile rheological phase method via two kinds of Fe sources of $FePO_4\cdot4H_2O$ and $FeC_2O_4\cdot2H_2O$, respectively. The as-obtained $LiFe_{0.5}Co_{0.5}PO_4$/C composites can be indexed as the typical olivine structure without impurity phase. Benefiting from the smaller average particle size and better dispersibility, the specific surface area of $LiFe_{0.5}Co_{0.5}PO_4$/C applying $FeC_2O_4\cdot2H_2O$ is up to 44 $m^2\cdot g^{-1}$, which implies a

higher interfacial contact area between the active particles and the electrolyte, as well as an increase in its capacitance capability. Besides, it has fine carbon coating effect with a uniform and full carbon layer of ~2.5 nm on the surface of nanoparticle, consequently resulting in enhanced electrical conductivity of materials and formation of a good protective layer between active material and electrolyte. Therefore, as cathode materials for LIBs, the sample via $FeC_2O_4 \cdot 2H_2O$ as Fe reactant exhibits more excellent electrochemical properties, *i.e.*, a high capacity of 137.5 $mAh \cdot g^{-1}$ at 0.1C and better cycle life. Based on this study, it is demonstrated that the great effect of Fe sources for the properties of $LiFe_{0.5}Co_{0.5}PO_4$/C composites. This report would provide critical guidance for the preparation of $LiFe_xCo_{1-x}PO_4$ solid solution materials.

Acknowledgements: This work acknowledges the support of the Research Foundation for the Postdoctoral Program of Sichuan University (Grant No.2017SCU12018) and National key research projects (Grant No.2017YFB0307504).

References:

[1] Goodenough J B, Park K S. *J. Am. Chem. Soc.*, **2013**,**135**(4):1167-1176

[2] Xie Y Y, Zhang W M, Gu S, et al. *Chin. J. Chem. Eng.*, **2016**, **24**(1):39-47

[3] Zhou L M, Zhang K, Hu Z, et al. *Adv. Energy Mater.*, **2018**, **8**(6):1701415

[4] XU Shan(徐杉), LU Lin(卢琳), LIU Lian(刘恋), et al. *Chinese J. Inorg. Chem.*(无机化学学报), **2016**,**32**(1):124-130

[5] ZHENG Zhuo(郑卓), YANG Xiu-Shan(杨秀山), HUA Wei-Bo(滑玮博), et al. *Chinese J. Inorg. Chem.*(无机化学学报), **2017**,**33**(6):963-969

[6] Eftekhari A. *J. Power Sources*, **2017**,**343**:395-411

[7] Padhi A K, Nanjundaswamy K S, Goodenough J B. *J. Electrochem. Soc.*, **1997**,**144**(4):1188-1194

[8] ZHANG Ying-Jie(张英杰), ZHU Zi-Yi(朱子翼), DONG Peng (董鹏), et al. *Acta Phys.-Chim. Sin.*(物理化学学报), **2017**, **33**(6):1085-1107

[9] DONG Jing(董静), ZHONG Ben-He(钟本和), ZHONG Yan-Jun(钟艳君), et al. *Chinese J. Inorg. Chem.*(无机化学学报), **2013**,**29**(10):2257-2264

[10]Bramnik N N, Nikolowski K, Baehtz C, et al. *Chem. Mater.*, **2007**,**19**(4):908-915

[11]Wang Y, Qiu J Y, Yu Z, et al. *Ceram. Int.*, **2018**,**44**(2):1312-1320

[12]Ornek A, Can M, Yesildag A. *Mater. Charact.*, **2016**,**116**:76-83

[13]Li J L, Wang Y, Wu J H, et al. *J. Alloys Compd.*, **2018**,**731**: 864-872

[14]Zhang H, Wei Z K, Jiang J J, et al. *J. Energy Chem.*, **2018**, **27**(2):544-551

[15]Wang H L, Yang Y, Liang Y Y, et al. *Angew. Chem. Int. Ed.*, **2011**,**50**(32):7364-7368

[16]Ding B, Xiao P F, Ji G, et al. *ACS Appl. Mater. Interfaces*, **2013**,**5**(22):12120-12126

[17]Gong C L, Xue Z G, Wen S, et al. *J. Power Sources*, **2016**, **318**:93-112

[18]Gong Z L, Yang Y. *Energy Environ. Sci.*, **2011**,**4**(9):3223-3242

[19]LUO Di-Di(罗迪迪), TIAN Jian-Hua(田建华), ZHU Xi(朱希), et al. *Chinese J. Inorg. Chem.*(无机化学学报), **2017**,**33**(6):1000-1006

[20]Wang Y M, Wang F, Feng X J. *J. Mater. Sci.-Mater. Electron.*, **2018**,**29**(2):1426-1434

[21]LIN Jian(林健), CUI Yong-Fu(崔永福), CUI Jin-Long(崔金龙), et al. *Chinese J. Inorg. Chem.*(无机化学学报), **2018**,**34**(1):33-42

[22]Wang J J, Sun X L. *Energy Environ. Sci.*, **2012**,**5**(1):5163-5185

[23]Share K, Westover A, Li M, et al. *Chem. Eng. Sci.*, **2016**, **154**:3-19

[24]Strobridge F C, Liu H, Leskes M, et al. *Chem. Mater.*, **2016**, **28**(11):3676-3690

[25]Ruffo R, Mari C M, Morazzoni F, et al. *Ionics*, **2007**,**13**(5): 287-291

[26]Wang D Y, Wang Z X, Huang X J, et al. *J. Power Sources*, **2005**,**146**(1/2):580-583

[27]Xing L Y, Hu M, Tang Q, et al. *Electrochim. Acta*, **2012**,**59**: 172-178

[28]Li H H, Jin J, Wei J P, et al. *Electrochem. Commun.*, **2009**, **11**(1):95-98

[29]Zhong Y J, Wu Z G, Li J T, et al. *ChemElectroChem*, **2015**, **2**(6):896-902

[30]Yan Z C, Liu L, Shu H B, et al. *J. Power Sources*, **2015**, **274**:8-14

[31]Wang X F, Feng Z J, Huang J T, et al. *Carbon*, **2018**,**127**: 149-157

[32]Zhang Q, Chen L, Huang C P, et al. *J. Mater. Sci.-Mater. Electron.*, **2016**,**27**(12):12649-12653

[33]Xiang J F, Chang C X, Zhang F, et al. *J. Alloys Compd.*, **2009**,**475**(1/2):483-487

[34]Huang X Y, Hu Q H, Liu J Q, et al. *Ionics*, **2017**,**23**(9):2269-2273

[35]Zhong Y J, Li J T, Wu Z G, et al. *J. Power Sources*, **2013**, **234**:217-222

[36]Shen H H, Xiang W, Shi X X, et al. *Ionics*, **2016**,**22**(2):193-200

[37]Wang Y Y, Tang Y, Zhong B H, et al. *J. Solid State Electrochem.*, **2014**,**18**(1):215-221

[38]Dong B, Huang X, Yang X, et al. *Ultrason. Sonochem.*, **2017**,**39**:816-826

[39]LI Wan-Long(李万隆), LI Yue-Jiao(李月姣), CAO Mei-Ling(曹美玲), et al. *Acta Phys.-Chim. Sin.*(物理化学学报), **2017**, **33**(11):2261-2267

[40]Maeyoshi Y, Miyamoto S, Noda Y, et al. *J. Power Sources*, **2017**,**337**:92-99

[41]Tan L, Luo Z M, Liu H W, et al. *J. Alloys Compd.*, **2010**, **502**(2):407-410

[42]Gao F, Tang Z Y. *Electrochim. Acta*, **2008**,**53**(15):5071-5075

[43]Liu T F, Zhao L, Wang D L, et al. *RSC Adv.*, **2014**,**4**(20):10067-10075

[44]Shu H B, Wang X Y, Wu Q, et al. *J. Power Sources*, **2013**, **237**:149-155

[45]TANG Yan(唐艳), ZHONG Yan-Jun(钟艳君), OU Qing-Zhu(欧庆祝), et al. *Acta Phys.-Chim. Sin.*(物理化学学报), **2015**,**31**(2):277-284